Discover Mechanical Engineering

Research

Application of digital twin technology in monitoring system of pump turbine

Qifei Li[1,2] · **Lu Xin**[1] · **Runtao Li**[1]

Received: 7 June 2024 / Accepted: 26 September 2024
Published online: 02 October 2024

Abstract
The advent of advanced productive forces has catalyzed the ongoing evolution of intelligent and digital technologies within the pump-turbine sector. The integration of digital technologies has not only enhanced production efficiency but also facilitated intelligent operation management, offering novel solutions for pump-turbine design and operation, thereby accelerating the digital transformation in fluid machinery. This study first established the theoretical framework of the digital twin system for pump-turbines, followed by the development of a mathematical model and the construction of a twin virtual model utilizing Proper Orthogonal Decomposition (POD) reduction theory. The model's accuracy was validated through real-time pressure pulsation data, and exploratory investigations into cavitation prediction were subsequently carried out. To enable the visualization of the digital twin system, this study incorporated Open3D (Three-dimensional computer graphics tools) point cloud technology, effectively rendering the state cloud map of the pump-turbine. Finally, by synthesizing the proposed theories and technologies, the digital twin system's visualization and monitoring for pump-turbines were successfully implemented through the Unity3D simulation platform. This study offers novel insights into intelligent monitoring and prediction of pump-turbines, holding significant implications for the modernization and intelligent advancement of the hydropower industry.

Keywords Digital twin · Pump-turbine · Reduced-order model · LSTM networks · Monitoring prediction

1 Introduction

With the concept of new quality productivity, digital twin technology has attracted much attention as a key tool to promote industrial transformation and upgrading. The integration of digital twin technology has unlocked fresh opportunities for industrial production, facilitating the intelligent and digital transformation of production processes and expediting the journey of industrial transformation and upgrading.

Pump-turbines have shown a trend of continuous development and progress in technology, intelligence, energy saving, environmental protection, multifunctionality and international cooperation, bringing more opportunities and challenges for hydropower generation and water resources utilisation. With China's robust development of wind and solar power generation, energy storage has become paramount [1, 2], leading to heightened efforts in constructing pumped storage power stations and increasing the utilization of pumped storage units. Pump-turbine are advancing towards higher and ultra-high heads, accompanied by increased flow rates. To enhance hydraulic efficiency, impeller blades are

✉ Qifei Li, lqfy@lut.edu.cn; Lu Xin, 441727334@qq.com; Runtao Li, 97394266@qq.com | [1]School of Energy and Power Engineering, Lanzhou University of Technology, Lanzhou 730050, Gansu, China. [2]Key Laboratory of Fluid Machinery and Systems, Lanzhou 730050, Gansu, China.

being made thinner. However, this thinning increases operational strain and blade amplitude [3], leading to heightened stress concentration at the blade inlet edge, upper crown, and lower ring. Pumped storage units play a vital role in the power system for "peak shaving and valley filling," necessitating both conventional hydropower generation functionality and energy storage tasks, thereby adding to design complexity. These units operate under diverse conditions, requiring multiple transitions within a day and sometimes occurring several times per hour. Operating under non-design conditions, the transition process of pump-turbine is complex, often accompanied by severe pressure pulsations, secondary flows, and flow instability phenomena. This may result in fluid–structure coupling vibration phenomena, triggering unit resonance, causing severe fatigue damage to the impeller, and posing a threat to the safe and stable operation of the entire unit or even the pumped storage power station [4].

The concept of digital twins originated in the 1960s to address issues in the design and operation of spacecraft [5–7], particularly to enhance their reliability and safety [8]. Scientists realized that data obtained during the design and testing phases might differ from real-world operational conditions. Thus, the concept of "digital twins" was proposed, aiming to create a virtual replica corresponding to the actual system through numerical models in computers, thereby achieving more accurate predictions of system behavior. China's "14th Five-Year Plan" also explicitly identifies digital twins and interaction as priority development areas, indicating that the future research on digital twins in China will flourish [9].

With the continuous advancement of computer technology and the growing maturity of numerical simulation methods, numerical twinning is increasingly applied across various fields including engineering, medicine, and economics [10]. Modern numerical twinning serves not only for optimizing design and predicting system performance but also for fault diagnosis, intelligent control, and other purposes. This concept's evolution and expansion offer industries opportunities to enhance and optimize workflow processes digitally. Professionals, scholars, and scientists across diverse fields have shown keen interest in developing and applying numerical twinning due to its potential in addressing complex problems and improving system efficiency. For example, Knapp et al. [11] developed and rigorously validated a digital twinning model for additive manufacturing processes, accurately predicting temporal and spatial variations of parameters influencing the structure and performance of metallurgical components. The OPTi project in Europe applies digital twinning technology to regional heating and cooling systems, utilizing consumer comfort zone estimation methods to reduce energy consumption and predict load peaks for preheating and precooling [12]. Amid the pandemic, Sabri et al. [13] utilized digital twinning technology to create a digital twin of a laboratory, enriching online teaching content. Digital twin laboratories, compared to traditional ones, can expand the number and functionality of experimental equipment, reduce experimental costs, and enable more students to participate in experiments.

At present, most of China's research is still at the beginning and catching up stage. For instance, Tao et al. [14–16] introduced the concept of digital twinning workshops, outlining their structure, operation, and key technical elements. They explored product design, production, and services influenced by digital twinning and big data, comparing them within the context of intelligent manufacturing and Industry 4.0. Additionally, Tao et al. [17] investigated digital twinning and its applications, proposing application guidelines and addressing key issues and technologies in 14 digital twinning-driven scenarios. Zhang et al. [18] presented an intelligent modeling approach based on Cyber-Physical Systems (CPS) for real-time monitoring and autonomous decision-making in smart factories. Zhang et al.[19] proposed a method for constructing a digital twinning model tailored to complex component assembly processes. Broo [20] suggested employing digital twinning to enhance infrastructure system efficiency. Guo [21] applied digital twinning for network optimization in controlling sixth-generation (6G) wireless technology. Song et al. [22] explored digital twinning applications in sustainable development for nuclear power plants, emphasizing real-time, high-precision simulation. Wang et al. [23] discussed combining digital twin technology with pumped storage power stations, foreseeing further development in digitalized units. Yin et al. [24] tackled insufficient monitoring of shield replacement robots through a digital twin-based system, verifying its effectiveness. Shi et al. [25] utilized digital twinning to predict the residual service life of continuous casting rollers, aiding intelligent operation and maintenance decisions. Wang et al. [26] proposed evaluating production plans through digital twin workshops to optimize workshop production plans based on actual simulated data. Liu [27] introduced a digital twin method for centrifugal pumps, combining CFD technology and data-driven compensation for equipment health maintenance and management digitization. Figure 1 demonstrates the application of digital twins in various domains.

In the realm of pump-turbine modeling and simulation, traditional theoretical analysis and experimental methods are increasingly insufficient to meet the demands of modeling complex mechanical structure flow fields. The current impeller mechanical fault diagnosis research methods, fault diagnosis methods are relatively single, based on virtual simulation and other diagnostic methods, by the pump-turbine fault characteristics, technical means and many other factors, there are greater limitations. While Computational Fluid Dynamics (CFD) technology has

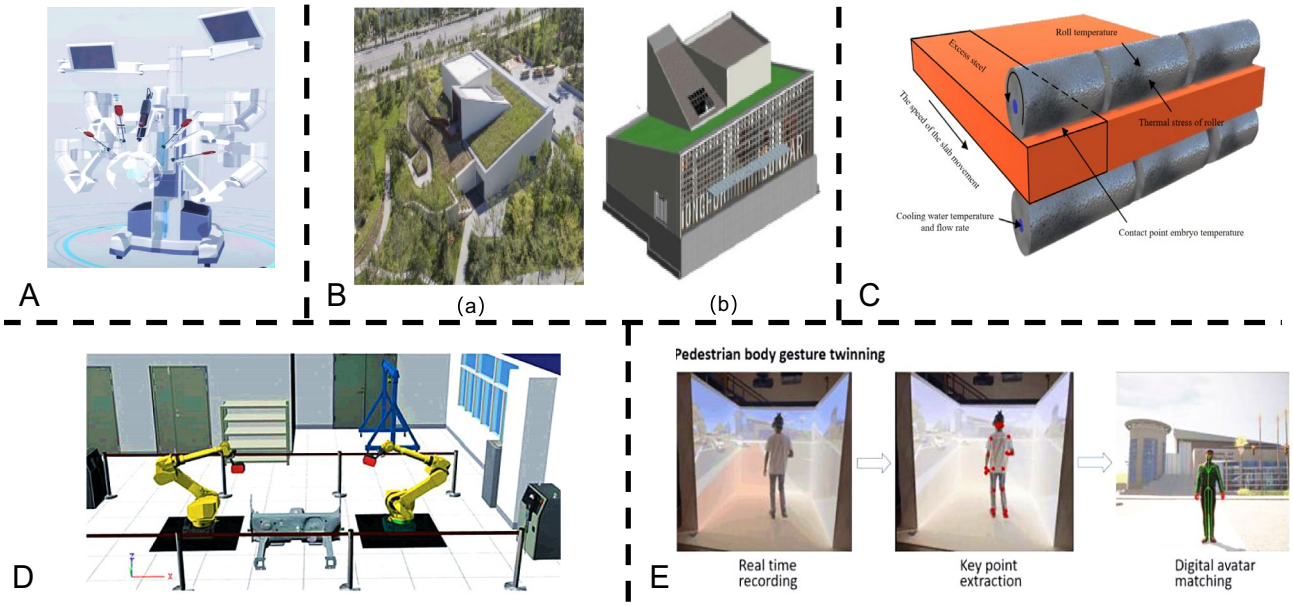

Fig.1 Applications of digital twinning span various domains, including **A** medicine [28], **B** architecture [29], **C** mechanical continuous casting machines [25], **D** Application of automotive on-line detection system [30] and **E** Application of intelligent transportation system [31]

introduced breakthrough technical capabilities, it still encounters challenges in independently supporting precise modeling of complex flow fields due to inherent technical constraints.

In recent years, digital twinning technology has garnered increasing attention as an interdisciplinary research application integrating multiple dimensions, physical parameters, and hierarchical simulation methods. It digitally maps the entire life cycle status of physical equipment or systems in physical space through digital twinning models in the digital realm. This technology finds widespread application in areas such as health management of production equipment and systems, as well as product design and manufacturing. However, the fault diagnosis of pump-turbine currently encounters various challenges, including the necessity for extensive damage experiments to acquire fault characteristic data, which is costly, time-consuming, and poses safety concerns. Moreover, the bidirectional operating conditions complexity of pump-turbine and the diverse nature of blade failures compound these challenges. Traditional fault diagnosis methods heavily rely on the experiential knowledge of maintenance personnel, resulting in slow feedback, inefficient diagnosis, and passive maintenance practices lacking precision. Digital twinning technology addresses these challenges by constructing digital twin models of physical entities, introducing virtual faults, employing model simulation to gather fault characteristic data, and offering virtual data sources for fault diagnosis algorithms. This approach introduces novel perspectives for fault characteristic generation and diagnosis methods.

This study designs and develops a pump-turbine monitoring system grounded in digital twin technology. The system leverages machine learning techniques to construct a mechanical data monitoring model, enabling rapid monitoring of parameters such as stress, deformation, and pressure pulsation across various operating conditions, thereby facilitating real-time monitoring of key parameters and accurate prediction of unit status. Ultimately, through the integration of theoretical frameworks and technical methodologies, a digital twin highly congruent with actual pump-turbine operating conditions was developed using the Unity3D platform. This research integrates digital twin technology with deep vision and other cutting-edge technologies to explore more intelligent methodologies for pump-turbine fault diagnosis and its practical applications. This research holds significant practical importance and application value in advancing the digital transformation of the hydropower industry and in enhancing the operation and maintenance management capabilities of hydropower stations.

2 Digital twinning framework for pump-turbine monitoring systems

Based on Tao Fei et al.'s five-dimensional model of digital twin theory [16] and tailored to the specific requirements of pump turbine engineering, the pump turbine monitoring system is structured into five layers: the object entity layer, data layer, virtual twin layer, application layer, and interconnections between these layers, as illustrated in Fig. 2.

2.1 Physical entity layer

The foundation of the digital twinning system is formed by the physical entity layer, comprising tangible entities. In the context of the pump-turbine monitoring system, these physical entities primarily encompass spiral casings, fixed guide vanes, movable guide vanes, impellers, draft tubes, and data acquisition devices like vibration sensors and flow meters. The experimental platform utilized for this investigation is located at the Key Laboratory of Hydraulic Power Equipment in Tianjin. Notably, the impeller region serves as the primary focus of monitoring within the pump-turbine system, while the data acquisition devices serve as the means for gathering twinning data, with real-time data transmission occurring through the connection layer [32].

2.2 Data layer

Accurate data collection and efficient transmission are pivotal determinants of real-time performance in twinning systems [33, 34]. The data layer of the pump-turbine monitoring system encompasses crucial aspects such as geometric dimensions, assembly relationships, and spatial positions among various components. Leveraging this dataset, three-dimensional modeling is achieved through specialized software, enabling spatial layout simulation within a virtual twinning environment. Moreover, real-time data captured during pump-turbine operation include key parameters like

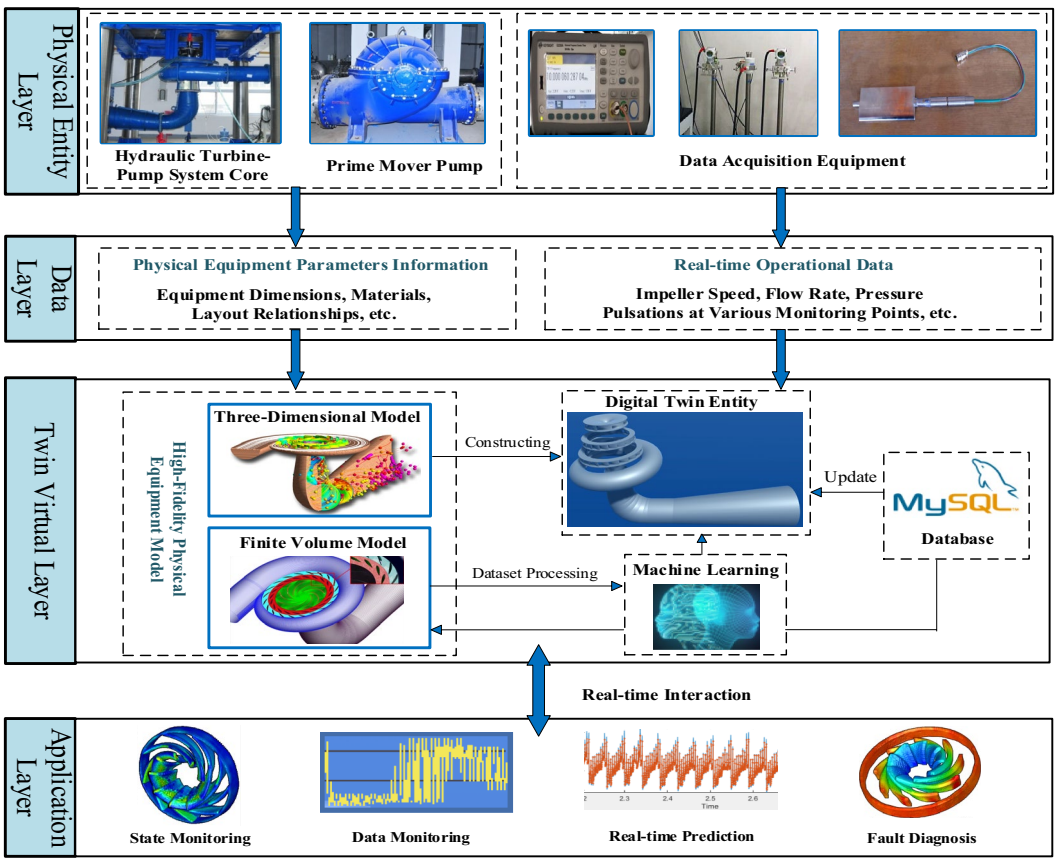

Fig. 2 Framework of intelligent pump-turbine monitoring system based on digital twinning

impeller speed, flow rate, head, and other operational metrics gathered by data acquisition devices. These datasets also encompass vital operational parameters such as vibration, temperature, and lubricating oil pressure. Such real-time data are instrumental in monitoring system operation status, fault diagnosis, and performance optimization.

2.3 Virtual twinning layer

The virtual twin layer serves as a digital counterpart mirroring the physical entity, established through a virtual simulation platform. Utilizing 3D modeling software like Creo, the 3D geometric model of the actual pump-turbine is created, maintaining fidelity to its real-world configuration. The finite volume model of the pump-turbine is then constructed to reflect its actual layout. Leveraging the Unity 3D development platform, the digital twin is fashioned according to the physical attributes of the real pump-turbine system, enabling the replication of physical space motion through twin data manipulation. Concurrently, various load inputs are factored in to swiftly capture the mechanical response of the pump-turbine via machine learning algorithms, thereby facilitating real-time monitoring of the model's mechanical data.

2.4 Application layer

The application layer, which builds upon the virtual twinning layer and aligns with practical application requirements, delivers relevant services and functionalities through intelligent algorithm and program encapsulation [35]. Within the pump-turbine digital twinning monitoring system, the application layer encompasses pivotal modules such as real-time monitoring, data panel display, and mechanical monitoring. Through the digital twinning entity, the real-time monitoring module tracks the pump-turbine's motion status, providing intuitive insights into key parameters. The data panel display module analyzes and presents data on the user interface, enhancing system visualization through graphical representations. Leveraging machine learning algorithms, the mechanical monitoring module swiftly acquires stress and deformation data from the impeller area, ensuring system safety and optimizing fault-handling capabilities. Additionally, the virtual reality interaction module facilitates real-time interaction via hardware devices, suitable for operational demonstrations and educational purposes, thereby enriching the system operation experience.

3 Construction of monitoring model based on unity3D

3.1 Overview of unity engine

The Unity engine, renowned for its cross-platform capabilities, finds extensive application across various domains including game development, virtual reality, augmented reality, and simulation training. Its robust features and intuitive interface empower developers to efficiently produce top-tier visual effects and interactive experiences. With support for multiple platforms, Unity enables seamless deployment of projects across diverse environments. Moreover, its extensive asset library and plugin ecosystem furnish developers with a wealth of tools and resources, thereby expediting the realization of creative concepts and project objectives.

Unity3D was selected as the development platform for the pump-turbine monitoring system. To synchronize the digital twin system with the hydro-turbine's motion in physical space, a kinematic model integrating virtual and real physical spaces was constructed. Utilizing virtual reality and panoramic roaming technology, the digital twin system's user interface interaction system was developed to deliver comprehensive monitoring capabilities, thereby enhancing interaction and visualization. Following requirement and technical analyses, the server-side was developed using the ASP.NET framework, while the client-side was based on the Unity engine, utilizing the MYSQL database. Further details regarding the specific hardware and software environment are provided in Table 1.

3.2 System for visual interaction

Utilizing physical space data, a three-dimensional model of the pump-turbine unit was constructed and seamlessly integrated into Unity3D. Real-time data transmission to Unity3D was facilitated by establishing a relational database using MySQL and Socket communication protocols. By employing C# scripts for parsing real-time motion data and applying kinematic equations, a dynamic linkage between the actual and virtual environments was established.

Table 1 Hardware and software environments

Hardware	Software	Development Environment Requirements
Central Processing Unit (CPU)	Operating System (OS)	Intel Core i9-13900 H Microsoft Windows 11
Random Access Memory (RAM)	Development Environment	32.00 GB Microsoft.Net Framework 4.0
Hard Disk Drive (HDD)	Programming Language	1 TB Matlab, Python, C#
Graphics Processing Unit (GPU)	Database Software	RTX 4090 Ti MYSQL 8.0

For comprehensive monitoring capabilities, a panoramic roaming system and an interactive interface leveraging virtual reality technology were devised. The panoramic roaming system allows exploration of products and spaces from a first-person perspective, with the ability to freely adjust observation positions within the virtual scene using standard PC peripherals. The UI interaction script, developed in C#, enables manipulation of observation positions and angles using keyboard directional keys and mouse scroll wheels, facilitating panoramic exploration of the pump-turbine unit. Concurrently, the VR interaction system immerses users in a lifelike three-dimensional simulation environment through virtual reality technology, delivering an engaging interactive experience.

4 Development of mechanical monitoring using pod-based reduced order model

When choosing the reduced-order model, the complexity of the pump-turbine operating conditions, the nonlinearity of the flow and the real-time requirement of the system are taken into account. Balanced Truncation (BT) is not suitable for rapid response due to the complexity of computation and large data requirement, and Reduced Basis Method (RBM) is difficult to cope with variable working conditions due to its poor flexibility. Therefore, the POD (Proper Orthogonal Decomposition) model is chosen as the core downscaling model in this study [36], which significantly reduces the computational complexity while maintaining high accuracy, is particularly suitable for real-time monitoring and condition prediction, and shows high consistency with CFD results in multiple validations.

4.1 Proper orthogonal decomposition

This study employs Proper Orthogonal Decomposition (POD). POD reduction method fundamentally entails extracting normalized orthogonal bases from available data sample sets. These orthogonal bases approximate the original data set, thereby achieving a low-dimensional representation of the original model. In the context of nonlinear systems with input–output relationships, such as CFD control equations, POD constructs the requisite reduced-order transformation matrix by selecting a set of experimental data sets, termed snapshots, to facilitate dimensionality reduction.

Assuming the input variable function of the research object as $u(t)$ and the output variable function as $z(x,t)$, where typically t denotes the time variable and x represents the spatial variable. Data on the parameter variations $x_i (i = 1, 2, \ldots\ldots, M)$ at each time t_j (j = 1, 2, ……, N) are collected from grid nodes and compiled into a snapshot output matrix, as shown in Eq. (1). This matrix encompasses a comprehensive set of node parameters such as static pressure, dynamic pressure, and flow rate.

$$U(x_i, t_j) = \begin{bmatrix} u(x_1, t_1) & u(x_1, t_2) & \cdots & u(x_1, t_N) \\ u(x_2, t_1) & u(x_2, t_2) & \cdots & u(x_2, t_N) \\ \vdots & \vdots & \vdots & \vdots \\ u(x_M, t_1) & u(x_M, t_2) & \cdots & u(x_M, t_N) \end{bmatrix} \tag{1}$$

The ultimate objective of Proper Orthogonal Decomposition (POD) is to represent the output variables as a finite sum in variable-separation form.

$$z(x,t) \approx \sum_{k=1}^{N} \lambda_k(t)\phi_k(x) \tag{2}$$

In the equation, $\lambda_k(t)$ represents the POD coefficients, which depend on the input variable function $u(t)$, and $\phi_k(x)$ represents the POD basis functions. N is the number of basis functions selected. As N approaches infinity, the approximation will tend to the exact value. When the POD basis functions are determined, the POD coefficients are uniquely determined.

Arrange $n \times m$ data snapshot into matrix $\mathbf{A}_{n\times m}$, where $\mathbf{A}_{ij}$ represents the *j-th* state variable in the *i-th* time step. This set of matrices is called a snapshot matrix, and its correlation matrix $\mathbf{A}\mathbf{A}^T \in \mathbf{R}^{n\times n}$ is a semi-positive definite matrix. Further transform the matrix into a deviation matrix $\widetilde{\mathrm{A}}$ of the mean value, so that

$$\widetilde{\mathbf{a}}_i = \mathbf{a}_i - \overline{\mathbf{A}}, i \in \{1, 2, ..., n\} \tag{3}$$

In the equation, $\mathbf{a}_i$ is the *i-th* row vector of $\mathbf{A}_{n\times m}$, $\widetilde{\mathbf{a}}_i$ is the *i-th* row vector of $\widetilde{\mathrm{A}}_{n\times m}$, and the elements in $\overline{\mathbf{A}}$ are the average values of all time steps $\overline{\mathbf{A}} = \frac{1}{n}\sum_{i=1}^{n} \mathbf{a}_i$.

When there is a set of orthogonal basis functions $\phi_i(x), i = 1, 2, ..., n$, such that $\frac{1}{n}\sum_{i=1}^{n} \left|\left\langle \widetilde{\mathbf{a}}_i, \phi_i \right\rangle_{L^2}\right|^2 \to \max$ and $\sum_{i=1}^{N} \left|\langle \phi_i, \phi_i \rangle_{L^2}\right|^2 = 1$, then $\phi_i(x), i = 1, 2, ..., n$ represents the optimal orthogonal basis functions to be solved. $\langle \cdot, \cdot \rangle_{L^2}$ denotes the typical inner product in the L^2-norm.

To identify this set of POD orthogonal basis functions $\phi_i(x), i = 1, 2, ..., n$, according to Sirovich's theory [37], the snapshot matrix $\widetilde{\mathrm{A}}$ can be subjected to SVD transformation, resulting in

$$\widetilde{\mathbf{A}} = \mathbf{U}\mathbf{\Sigma}\mathbf{V}^T \tag{4}$$

In the equation, $\mathbf{U} \in \mathbf{R}^{n\times n}$ and $\mathrm{V} \in \mathbf{R}^{m\times m}$ are orthogonal matrices composed of orthogonal vectors from $\widetilde{\mathbf{A}}\widetilde{\mathbf{A}}^T$ and $\widetilde{\mathbf{A}}^T\widetilde{\mathbf{A}}$ respectively. $\sum$ is a diagonal matrix of size $n \times m$. Due to $n \gg m$, its diagonal elements $\sum_{ii}$ consist of m non-negative numbers σ_i arranged in descending order, denoted as $\sigma_1 \geq \sigma_2 \geq \ldots \geq \sigma_m \geq 0$, which are referred to as the singular values of $\widetilde{\mathbf{A}}\left(\widetilde{\mathbf{A}}^T\right)$

.

For Eq. (4), let $\mathbf{U}\mathbf{\Sigma} = \mathbf{Q}$, resulting in $\mathbf{Q} \in \mathbf{R}^{n\times m}$, and $\widetilde{\mathbf{A}} = \mathbf{Q}\mathbf{V}^T$. Let $\mathbf{Q} = \{\mathbf{q}_1, ..., \mathbf{q}_k, ..., \mathbf{q}_m\}$, $\mathbf{V} = \left\{\mathbf{v}_1, ..., \mathbf{v}_k, ..., \mathbf{v}_m\right\}$

$$\widetilde{\mathbf{A}} = \mathbf{Q}\mathbf{V}^T = \sum_{k=1}^{m} \mathbf{q}_k\mathbf{v}_k^T \tag{5}$$

For Eq. (2), the output variable function $z(x, t)$ is represented by the snapshot matrix $\widetilde{\mathrm{A}}$, the coefficient matrix $\lambda_k(t)$ is represented by column vectors $\mathbf{q}_k$, and the orthogonal basis functions $\phi_k(x)$ are represented by row vectors $\mathbf{v}_k^T$.

4.2 POD reduction based on the Galerkin method

For $\widetilde{\mathrm{A}}$. Further implement low-rank approximation, for any r < m, set $\sigma_{r+1} = \sigma_{r+2} = \ldots = \sigma_m = 0$ in $\sum$ and obtain matrix $\sum_r$, which can be used to calculate the optimal r rank approximation of the snapshot matrix.

$$\widetilde{\mathbf{A}} \approx \widetilde{\mathbf{A}}_r = \mathbf{U}\mathbf{\Sigma}_r\mathbf{V}^T \tag{6}$$

Typically, the first r columns of matrices $\mathbf{U}$ and V are replaced with the original matrix, and $\sum_r$ is replaced with its main submatrix $r \times r$. The optimal basis set of size r corresponds to the functions composed of the largest r singular values (i.e., the first r columns of $\mathbf{U}$), at which point there are no other sets of rank r basis vectors closer to the Frobenius norm of the snapshot matrix $\widetilde{\mathrm{A}}$. The first r columns of matrix V provide the optimal orthogonal basis for approximating the data via POD, satisfying both optimality conditions and minimizing errors [38].

The quantity loss induced by the r vectors in the POD expansion set can be assessed through the rth order energy ratio:

$$I(r) = \sum_{j=1}^{r} \sigma_j^2 / \sum_{j=1}^{m} \sigma_j^2 \tag{7}$$

In the equation,σ_j represents the *j-th* singular value. Assuming $I(r) \geq d\%$, it indicates that the *r*-dimensional POD basis vectors $\{\phi_i\}_{i=1}^{r}$ retain *d*% of the information in the snapshot samples. As *r* approaches *m*, the value of I will tend to 1, which means no information loss. Take $I(r) \geq 99\%$, then any moment of the flow field variable can be represented as

$$z(x,t) = \overline{z}(x) + \sum_{k=1}^{r} \lambda_k(t)\phi_k(x) \tag{8}$$

In the equation, $\overline{z}(x) = \overline{\mathbf{A}}$ represents the average value of the spatial variables of the flow field, and $\sum_{k=1}^{r} \lambda_k(t)\phi_k(x)$ represents the reduced-dimensional space formed by a linear combination of a set of m basis functions.

For non-stationary numerical models of flow fields, in order to determine the POD temporal coefficient function $\lambda_k(t)$, the Galerkin method is applied to project the modal equation into the reduced-dimensional space $\mathbf{\Phi} = \{\phi_i | i = 1, ..., r\}$ expanded by POD basis functions, and eventually obtain the reduced-order model of POD.

4.3 Implementation of the reduced-order model for the turbine runner of the pump-turbine

Within the ANSYS digital twin framework, reduced-order models play a pivotal role in optimizing the complexity of system dynamic modeling, particularly in CFD simulations. These models transform 3D CFD simulations into one-dimensional mathematical representations, constituting a data-driven approach for reducing model dimensionality. Through data matrix decomposition and eigenvalue analysis, this method extracts primary motion patterns and structural features of the system, facilitating effective monitoring and analysis of the pump-turbine's turbine runner. Moreover, the reduced-order model substantially enhances computational efficiency, decreasing system response time from minutes or hours to seconds (or even milliseconds). This enhancement is critical for real-time simulation and large-scale system analysis within digital twin systems. Furthermore, the reduced-order model offers a convenient means for stability analysis, simplifying the evaluation of system stability and response under diverse conditions, thereby presenting a viable approach for stability optimization within digital twin systems.

To achieve this objective, a methodology is proposed wherein a design space is initially constructed, followed by solving the full-order model at multiple sample points within this space to gather data. Subsequently, machine learning techniques are applied to develop a streamlined turbine model, as illustrated in Fig. 3. In constructing efficient models, finite element or finite volume methods are typically utilized, with a focus on incorporating maximum physical information for the utilization of simplified models. Moreover, accelerated simulations of various fixed points can be employed to obtain simulation data not encompassed during the training phase. The roadmap for CFD model reduction is delineated in Fig. 4.

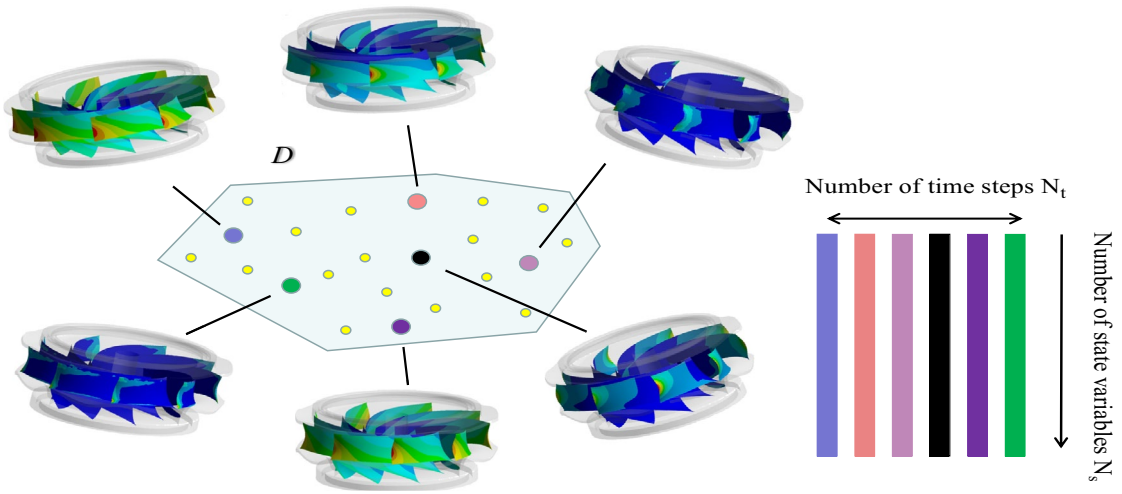

Fig. 3 Principle of Constructing POD Reduced-Order Model

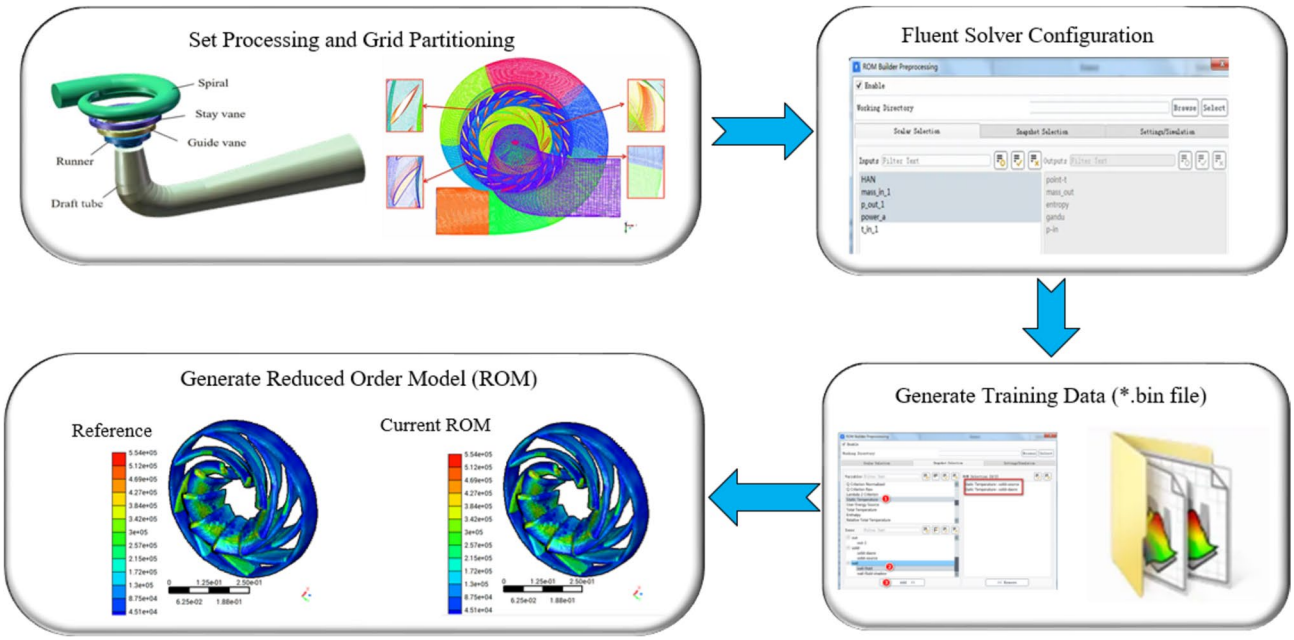

Fig. 4 Roadmap for 3D CFD Reduced-Order Model

4.4 Pressure fluctuation prediction algorithm based on long short-term memory (LSTM)

In recent years, deep learning has emerged as a leading machine learning technique, adept at autonomously extracting fault features from raw data. Prominent deep learning architectures like Convolutional Neural Networks (CNN) and Recurrent Neural Networks (RNN) have demonstrated successful applications across domains including computer vision, natural language processing, mechanical fault diagnosis, and more. Deep learning offers substantial improvements in diagnostic accuracy compared to conventional intelligent methodologies [39].

Long Short-Term Memory (LSTM) constitutes a specialized deep learning model tailored for processing sequential data, particularly adept at modeling and predicting time series data. Compared to conventional recurrent neural networks, LSTM networks demonstrate superior performance in handling long sequence data by mitigating issues like vanishing and exploding gradients. Comprising three "gate" structures and two state values, LSTM efficiently extracts long and short-term features separately by regulating the retention and omission of feature information across different time steps. The unit module structure, depicted in Fig. 5, illustrates the input x_t at time step t, with f, i, and o denoting the forget gate, input gate, and output gate respectively. By controlling these gates, the model effectively captures and retains long-term dependencies within sequential data, thus enhancing predictive accuracy. The learnable weights of corresponding gate structures are represented by W_m and m $\in \{f,i,c,o\}$, while tanh and $\boldsymbol{\sigma}$ signify the non-linear activation functions. Furthermore, $\otimes$ and $\oplus$ denote the Hadamard product and element-wise addition, with arrows indicating the direction of data flow. The long-term memory state at time step t within the grid structure is denoted by c_t, whereas h_t represents the short-term memory state and output at time step t.

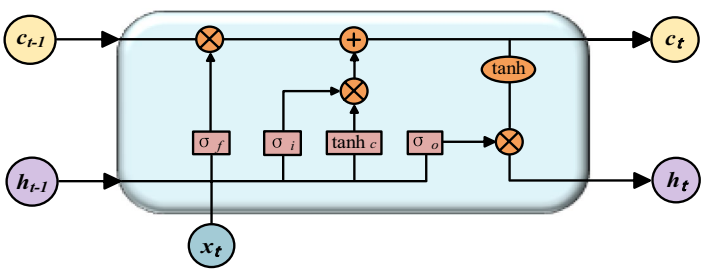

Fig. 5 Structure of LSTM Unit Module

In pressure pulsation prediction, the Long Short-Term Memory (LSTM) algorithm leverages historical data sequences to discern underlying patterns, enabling precise forecasts of future pressure pulsations. Compared to traditional time series forecasting methods, LSTM offers several advantages in this domain. Firstly, it adeptly captures long-term dependencies within data, resulting in more stable and dependable predictions. Secondly, it exhibits robust adaptability, accommodating various pressure pulsation data types. Furthermore, LSTM facilitates parameter learning via a back-propagation algorithm, enabling automatic feature and pattern acquisition from the data, thus automating feature design. By modeling sequences, LSTM assimilates temporal pressure pulsation characteristics, utilizing memory units to retain past information, thus enabling accurate modeling of dynamic pressure pulsation changes. Its unique gating mechanism facilitates effective handling of long sequence data, accurately capturing dynamic patterns and periodic fluctuations, and adapting to intricate, nonlinear pressure pulsation variations.

4.5 Implementation of cloud map based on open3d point cloud

The POD reduced-order model described in Sect. 3.1 efficiently acquires crucial physical parameters but lacks the capability for direct visualization of output cloud maps within Unity3D, a functionality commonly available in finite element simulation software such as ANSYS. To address this limitation, a cloud mapping feature based on open3d point cloud was introduced. Point cloud, which includes spatial structure and surface feature descriptors, is widely used in CAD modeling and rendering. Therefore, the point cloud approach was employed to visualize the prediction results of the reduced-order model. Each point in the point cloud contains the following information:

$$\text{Point} = (x, y, z, R, G, B) \tag{9}$$

The first three items denote the point's coordinate values in the spatial coordinate system, aligning with the node coordinates in the reduced-order model. Meanwhile, the last three items encompass the point's color information, with distinct colors reflected through varying values.

To mitigate the issue of point cloud voids within the dataset, a strategy is proposed to address this challenge by augmenting points. This entails leveraging ANSYS software to partition the modeling object into a denser grid, thereby obtaining surface node coordinates. These coordinates serve as input parameters to compute the stress and displacement of each point. Consequently, this method effectively augments the density of point cloud data, diminishes the impact of voids, and aligns with the real-time demands of the digital twin system. Given that the mainstream point cloud processing SDK Open3d offers a rich array of point cloud processing algorithms and boasts an efficient Python interface, while the Unity3D development engine primarily supports C# and JavaScript languages, implementing point cloud effects within Unity3D presents notable challenges. Hence, the mechanical monitoring system adopts Open3d for authoring point cloud processing programs. Moreover, it integrates the Python Scripting module within the Unity editor to facilitate real-time data transmission from the database to the Unity engine. This integration enables the invocation of Python point cloud code to realize mechanical monitoring effects. Fig. 6 shows the flow diagram of this pump-turbine digital twin system cloud diagram realization.

5 Experimental results and case analysis

5.1 Analysis of reduced order model accuracy

5.1.1 Comparison of accuracy of reduced order model pressure

In the field of pressure prediction, different models and methods can produce different results for runner blade pressure distribution. And the accuracy will also provide a seminal role for subsequent in-depth studies. For the Pod step-down model generated above, it is necessary to analyse the output results of the runner pressure for the traditional CFD model and the POD-based step-down model and analyse the error region in order to explore the accuracy of the step-down model in the prediction of the pressure cloud diagram.

Figure 7 presents a comparative analysis of pressure contour maps generated by the two models. The CFD simulation delivers precise pressure distribution, adept at capturing intricate flow phenomena. In contrast, the POD reduced-order model employs dimensionality reduction techniques to streamline prediction outcomes, offering concise yet effective

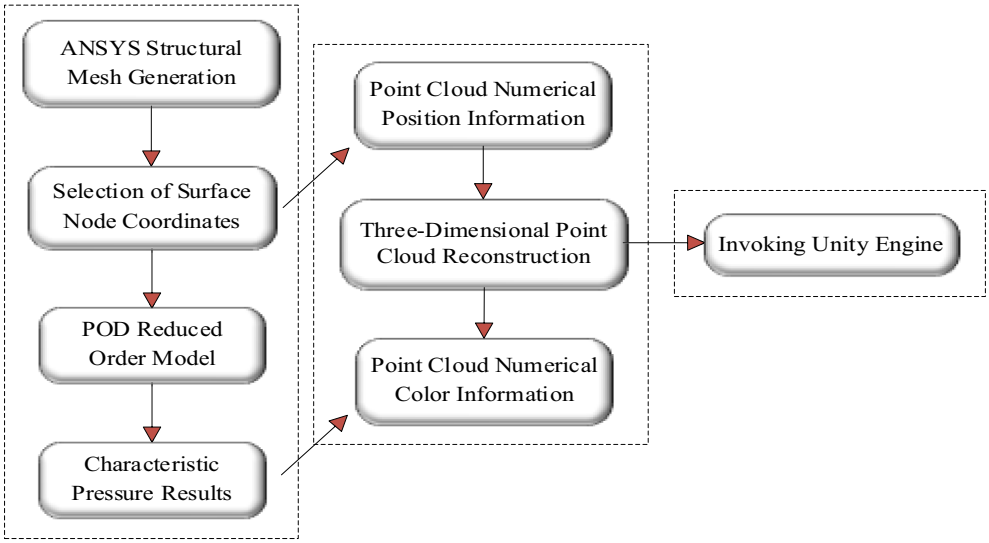

Fig. 6 Drawing Finite Element Cloud Diagram for Virtual Entities

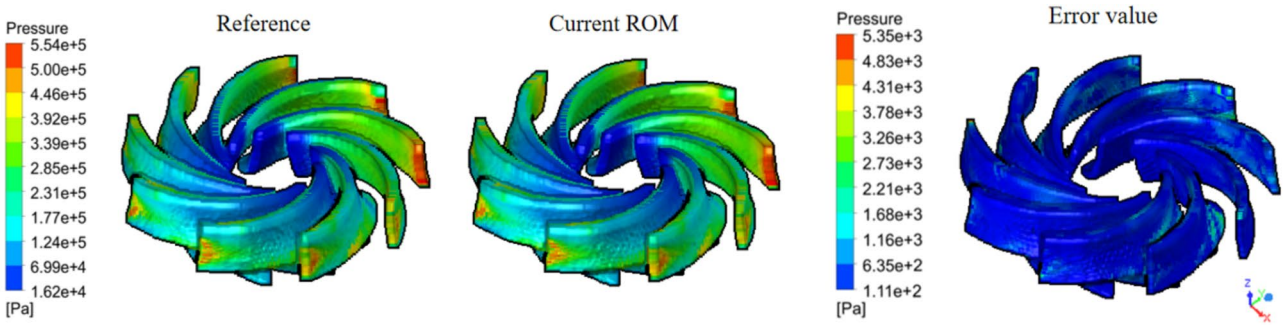

Fig. 7 Comparison and Error Region of Pressure between CFD Model and POD Reduced Order Model

results. Both models exhibit high consistency in overall trends, adept at capturing pressure fluctuations on turbine blades during operation. Notably, the inlet region experiences notable water flow impact, leading to elevated pressure points, while pressure gradually diminishes from outer to inner regions, aligning with turbine blade behavior under operational conditions.

Nonetheless, the prediction outcomes of the POD reduced-order model also display deviations from the CFD model, particularly in localized regions characterized by significant pressure variations. However, the highest relative error value observed is merely 0.9%. The discrepancies in the CFD model primarily stem from factors like grid partitioning and turbulence model selection, whereas those in the POD reduced-order model are chiefly influenced by modal truncation and data reconstruction accuracy.

5.1.2 Comparison of efficiency and accuracy of reduced-order models

This study establishes a highly simulated POD-based reduced-order model to efficiently simulate fluid dynamics behavior under experimental conditions. The model's performance is thoroughly evaluated with a focus on efficiency, primarily through metrics such as computational speed, time, and resource utilization. By meticulously comparing these metrics, the model's computational efficiency under simulated experimental conditions is comprehensively understood, aiding in validating its accuracy and providing crucial references for practical engineering applications. Furthermore, the model's robustness under various conditions is analyzed to assess its stability and applicability in real engineering environments. This comprehensive evaluation, considering both efficiency and robustness, lays a solid foundation for further research and applications.

Using the established POD reduced-order model, operational data such as pump and water turbine torque under specified conditions were obtained through solving. The weighted efficiency table for CFD and POD models is presented

Table 2 Verification table for weighted efficiency of pump-turbine

	Unit speed	Unit discharge	Prototype power	CFD efficiency	POD efficiency	Efficiency variance
	n_{11} (r/min)	Q_{11} (m^3/s)	P_p (MW)	η_p (%)	η_{hm} (%)	$\Delta\eta$ (%)
50%N	0.443	55.83	127.1	84.4	82.14	2.26
60%N	0.510	55.83	153.3	88.6	86.29	2.31
70%N	0.579	55.83	178.8	91.0	88.65	2.35
80%N	0.654	55.83	204.5	92.1	89.81	2.29
90%N	0.723	55.83	229.9	93.8	91.57	2.23
100%N	0.800	55.83	255.5	94.0	91.78	2.22

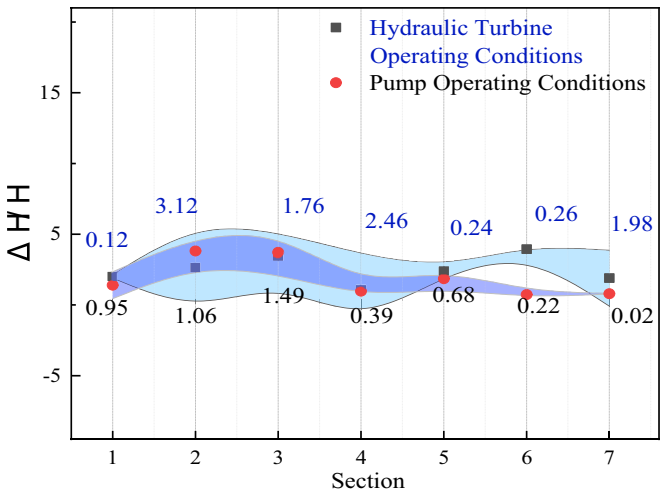

Fig. 8 Comparison of pressure pulsation between turbine and pump conditions

in Table 2. Notably, the difference in efficiency between experiments and models is less than 2.35% across the output range of 50%N to 100%N, showcasing the model's excellent robustness under varying outputs. Despite the prototype pump-turbine's efficiency exceeding that of the created model, the established POD reduced-order model still offers relatively accurate results, thereby facilitating engineering applications and analysis.

5.1.3 Comparison of accuracy of pressure pulsation in reduced-order models

Pressure pulsation within the internal flow field serves as a critical indicator for assessing unit stability, necessitating prediction and analysis in pump-turbine scenarios. Consequently, reliability verification of pressure pulsation values for both the reduced-order model and experimental setups is imperative. Detailed numerical values are depicted in Fig. 8, where regions one to seven correspond to specific locations within the flow domain, including the volute inlet, bladeless area, gaps between the top cover and impeller, and various sections of the draft tube. Experimental data reveal that, across the entire flow domain, errors are relatively pronounced in regions corresponding to the bladeless area and gaps between the top cover and impeller, with a pressure pulsation fluctuation error ($\Delta H{\cdot}H^{-1}$) of 3.12. Nonetheless, the numerical values of experimental results generally fall within an acceptable range. Consequently, it is concluded that the pressure pulsation predictions of the POD reduced-order model demonstrate high reliability at this stage.

Following the verification and comparison of computational accuracy between CFD simulations and the POD reduced-order model, the discussion shifts to the computational efficiency of the reduced-order model. As this study primarily focuses on monitoring the pump-turbine under off-design conditions, a comprehensive set of transient CFD simulations for such conditions was conducted. These simulations were executed on a server equipped with 72 cores and 144 threads, consuming approximately 195 h. The POD reduction and coefficient determination processes required approximately 28 h, constituting a one-time operation without the need for rebuilding the reduced-order model during subsequent applications. Notably, computational tasks using the POD reduced-order model were completed within 4 h and 22 min, showcasing a significant enhancement in computational efficiency. Consequently, the efficiency of solving transient problems using ROM methods is deemed remarkably high.

5.2 Prediction of pressure pulsations during load rejection conditions

Load shedding operations become more prevalent when there are fluctuations in demand or temporary issues within the system housing the pump-turbine.These operations involve rapid load reduction or shutdown, often leading to significant pressure fluctuations. Such fluctuations pose risks of system instability and equipment damage, potentially resulting in severe accidents. Therefore, accurately predicting pressure fluctuations during load-rejection events is critical. Predictive modeling allows for early identification of potential risks, enabling proactive implementation of control measures to maintain stable operation of pump-turbine systems. This proactive approach mitigates the risk of equipment damage and accidents, thereby enhancing production safety and equipment reliability.

Pressure pulsation prediction experiments were conducted using a specific pump-turbine's load rejection operation as a case study. The pump-turbine operates across various regions, including the pump, pump brake, turbine, turbine brake, and reverse pump regions, as depicted in Fig. 9. Due to the substantial impeller diameter and significant centrifugal force, the water flow velocity experiences a sharp decline, leading to a rapid downward bend in the characteristic curve, forming an "S" shape with a slight angle relative to the best efficiency point line. Within the "S" characteristic region, a single unit speed may correspond to multiple unit flow rates, including flow entering the reverse pump region. Under these circumstances, the pump-turbine is susceptible to transitioning directly from the best efficiency point to the reverse pump condition, potentially subjecting the unit structure to shock loads and risking damage to overflow components [40]. Additionally, the interaction between the impeller and water flow induces intense pressure pulsations, which could pose challenges for the unit to synchronize with the grid. Thus, predicting and analyzing pressure pulsations during load rejection operations are crucial.

Figure 10 illustrates the significant variation in speed and flow rate under load rejection conditions, resulting in highly volatile changes in the pressure pulsation curve spanning a considerable range of pressure values. This scenario provides an ideal case for evaluating the accuracy of LSTM pressure pulsation prediction algorithms. Numerical simulations are employed to comprehensively replicate the entire load rejection process of the pump-turbine, with a focus on selecting pressure pulsation values in the bladeless region for preparation for pressure pulsation prediction.

Figure 11 presents the LSTM prediction results for pressure pulsations, showcasing its exceptional capability in capturing long-term dependencies in time series data. Even amidst complex conditions like load rejection, the pressure pulsation data reveals intricate temporal dynamics, achieving a prediction accuracy of 95.95% for pulsation values and a mean absolute error (MAE) of 6.81, which represents only 1.32% of the average pulsation pressure. Pressure pulsation data, influenced by various factors, exhibits nonlinear changes and temporal variability, which have been effectively captured through extensive data analysis. This approach automatically learns crucial features in the data and applies them adeptly to prediction tasks, streamlining the modeling process while enhancing the model's generalization ability. Furthermore, a strong linear relationship is observed between changes in pulsation data and other variables, with a

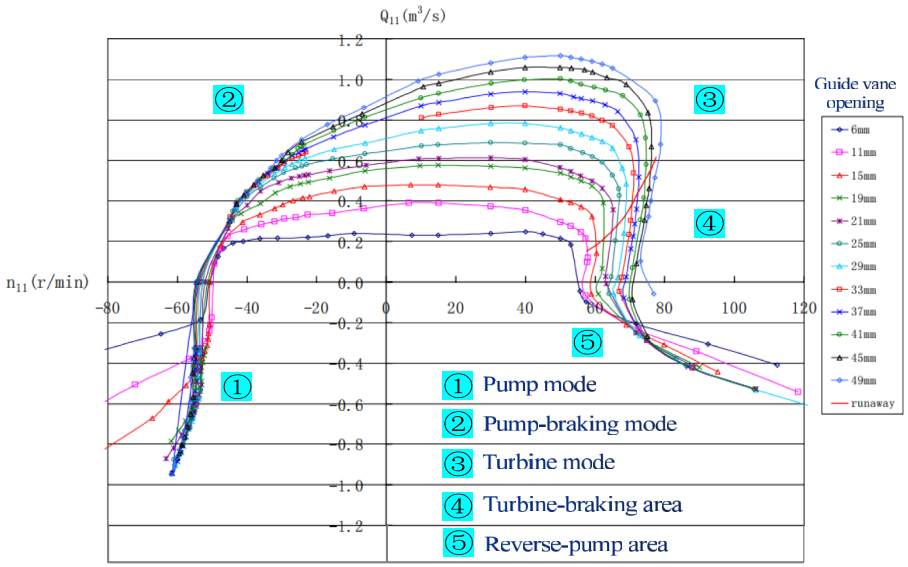

Fig. 9 Overall performance curve of pump-turbine

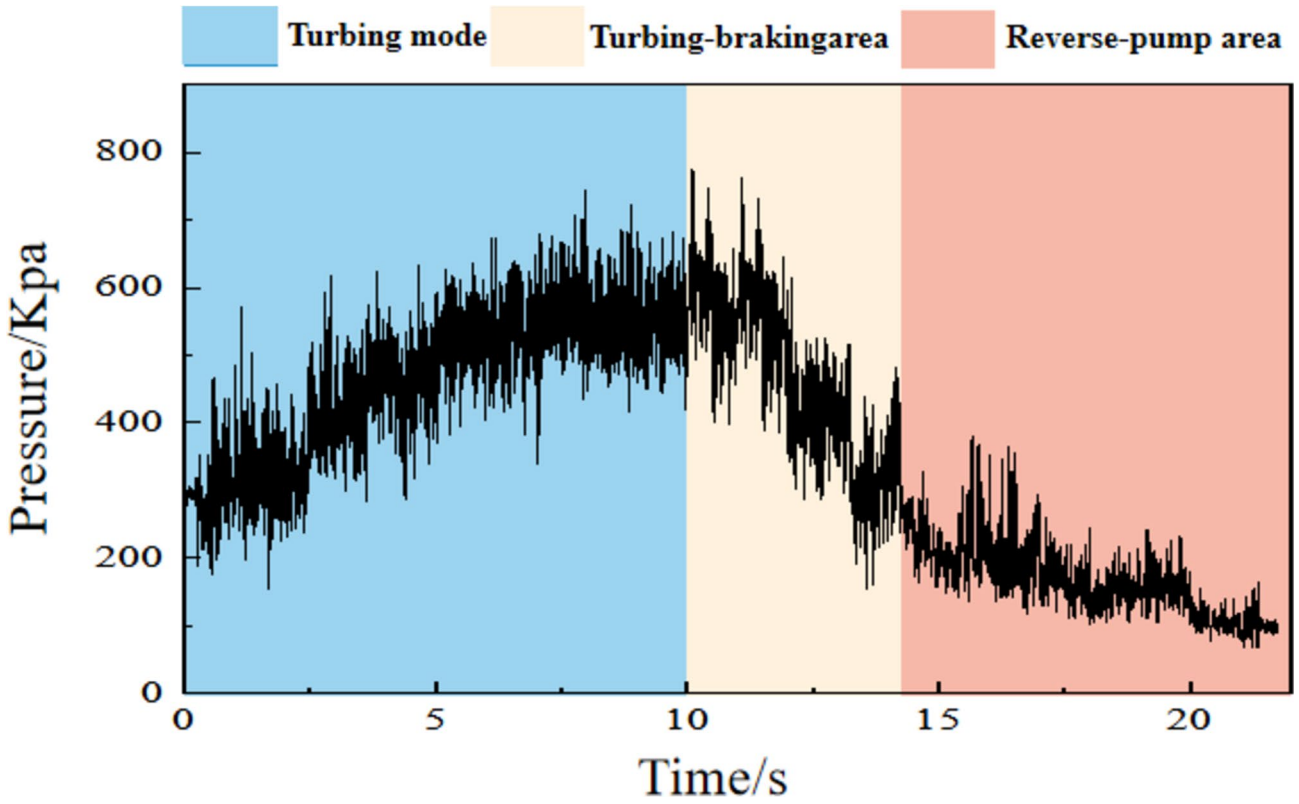

Fig. 10 Pressure pulsations in the bladeless region during load rejection process

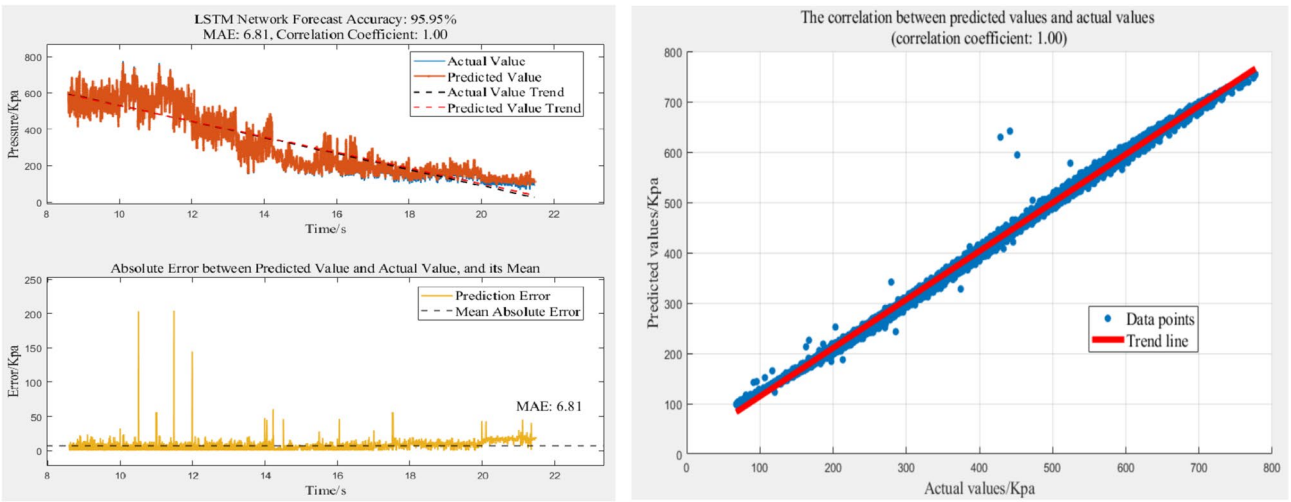

Fig. 11 Results of pressure pulsation prediction by LSTM model

correlation coefficient of 1.00, indicating precise capture and prediction of all data changes by the method employed in this study. The predicted pulsation curves closely align with the actual trends, thereby bolstering the accuracy and robustness of the model's predictions.

Moreover, the correlation coefficient of 1.00 in the prediction results attests to the presence of deterministic patterns or mechanisms in the pressure pulsation data during pump-turbine load rejection. By delving deeper into the origins and influencing factors of this correlation, a more profound comprehension of the operational mechanism during the load rejection process of pump-turbine can be garnered. This, in turn, enables the formulation of more precise and efficient control strategies to enhance unit performance optimization.

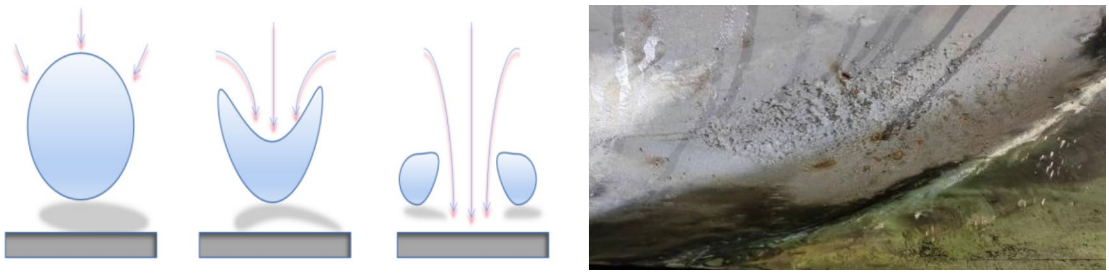

Fig. 12 Illustration of cavitation phenomenon and blade damage

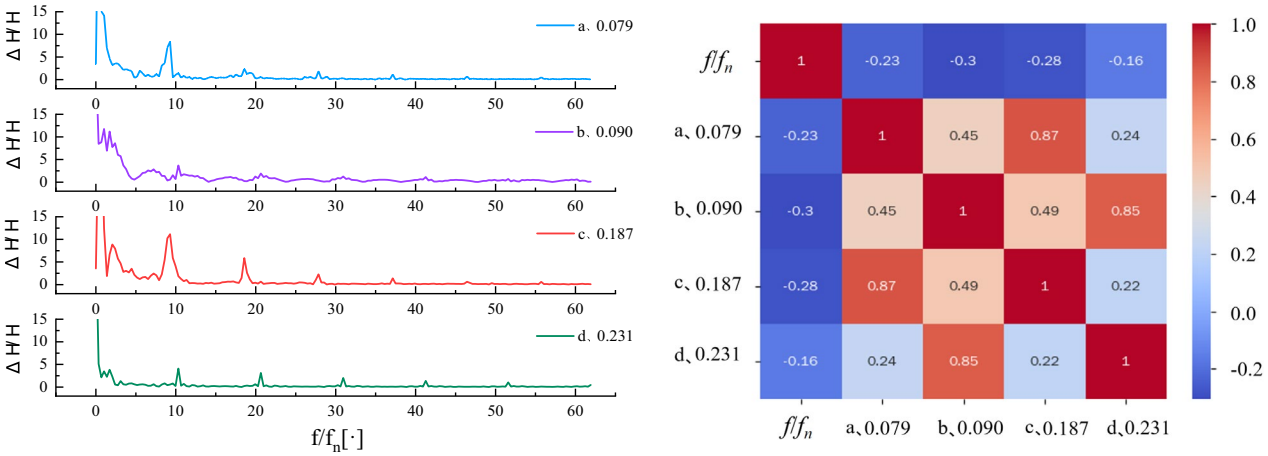

(a) Frequency domain plot (b) correlation matrix plot.

Fig. 13 Frequency domain plot of pressure pulsation and matrix plot

5.3 Anti-prediction of sparseness coefficient based on frequency domain features

Cavitation, characterized by the formation of gas bubbles or vapor within a liquid, is a common occurrence in fluid flow dynamics. Figure 12 visually depicts the cavitation phenomenon alongside blade damage. The detrimental effects of cavitation on pumps turbines primarily include reduced performance, heightened vibration, and equipment damage. These manifestations lead to diminished fluid transmission efficiency, increased equipment vibration and noise levels, and the potential erosion of blades, ultimately resulting in energy inefficiency and shortened equipment lifespan [41]. Hence, accurate assessment and monitoring of cavitation levels are imperative for ensuring optimal equipment operation.

Conventional monitoring techniques, often reliant on empirical knowledge or rule-based approaches, frequently exhibit shortcomings in accuracy and reliability. With the progression of digital twin systems, the ability to simulate and forecast equipment operational states with enhanced precision has become attainable. These systems, grounded in both physical models and data-driven methodologies, offer the capacity to faithfully replicate equipment behavior and perform predictive optimization leveraging real operational data.

To improve the predictability of cavitation incidents in pump-turbine, digital twin systems will be utilized for frequency domain feature analysis. Initially, pressure pulsation data corresponding to different cavitation coefficients and impeller positions will be collected as the focal point of investigation. Subsequently, leveraging the data processing capabilities of digital twin systems, feature extraction and analysis will be performed following frequency domain transformation. Emphasis will be placed on discerning characteristic features associated with varying degrees of cavitation, including frequency distribution, amplitude fluctuations, and waveform patterns. This analysis aims to provide deeper insights into the impact mechanism of different cavitation levels on pressure pulsations, thereby furnishing a more precise foundation for cavitation prediction. The frequency domain plot of pressure fluctuations is presented in Fig. 13a. The correlation matrix hotspot diagram is shown in Fig. 13b.

Pressure fluctuation characteristics exhibit slight variations under different cavitation coefficients. High-frequency components display heightened amplitudes, with the first dominant frequency signal consistently appearing at 9fn (blade passing frequency). The sub-frequency at 20fn (vane passing frequency) arises from fluid excitation force fluctuations due to impeller rotation and static interference from the fixed double-row vane grid. Additional low-frequency components, such as 5fn, contribute to compact, small-amplitude fluctuations within the frequency spectrum. Notably, visual patterns in the frequency domain plot do not directly elucidate significant correlations, necessitating statistical analysis of the collected data.

A heatmap of the correlation matrix was generated through frequency domain numerical computations to facilitate further data analysis. Within the correlation matrix, each cell represents the correlation coefficient between the variables denoted by the rows and columns. In this heatmap, darker colors indicate stronger correlations. The squares on the diagonal represent the correlation of a variable with itself, so their values are always 1.The graph illustrates that the amplitude at cavitation coefficient 0.09 exhibits the strongest correlation with harmonics, at 0.59.However, the correlations between the amplitude at cavitation coefficient 0.079, 0.187, and 0.231 and harmonics are slightly weaker, at 0.27, 0.31, and 0.35, respectively. This correlation matrix assists in identifying which features are most relevant to the desired prediction of cavitation coefficients and subsequently in establishing and predicting models for the data.

The inverse prediction method proves highly practical, particularly in scenarios where direct measurement of cavitation coefficients is challenging or necessitates real-time monitoring. Analyzing pressure pulsation signals allows for the identification of features correlated with cavitation coefficients, facilitating the establishment of predictive models for these coefficients. Such an approach enhances real-time monitoring and prediction capabilities for pump-turbine systems, enabling early detection of potential issues and the implementation of necessary measures to ensure system safety and reliability.

5.4 Visualization implementation of pump turbine digital twin systems.

To validate the effectiveness of the pump-turbine monitoring system, a simulated experimental scenario is devised leveraging the digital twin of the pump-turbine rotor system. Real-time data generated during actual pump-turbine operation is simulated using a serial port testing tool. The virtual prototype and serial port testing tool are interconnected through communication protocols like Socket, with the Unity virtual prototype functioning as the client.

Figure 14a illustrates the primary interface of the pump-turbine monitoring system, offering users the option to toggle between monitoring different modules such as stress, deformation, and pressure pulsation via buttons located at the top of the interface. The pump-turbine are synchronized with the physical space model within the data-driven digital twin system, enabling users to freely switch observation perspectives and positions using keyboard arrow keys and mouse scroll wheel, thus enabling panoramic roaming functionality. To provide an intuitive understanding of the operational status of the pumped storage unit, the monitoring subsystem can present real-time changes in key operational data. Figure 14b exhibits the real-time pressure pulsation curve and data of the turbine impeller blades and tailrace area during the operation of the pumped storage unit. The page data display panel can instantaneously exhibit data transmitted by physical entities, enabling visual real-time monitoring of operating condition changes.

(a) main interface of the twin system. (b) Monitoring interface of the twin system

Fig. 14 Operation of digital twin systems

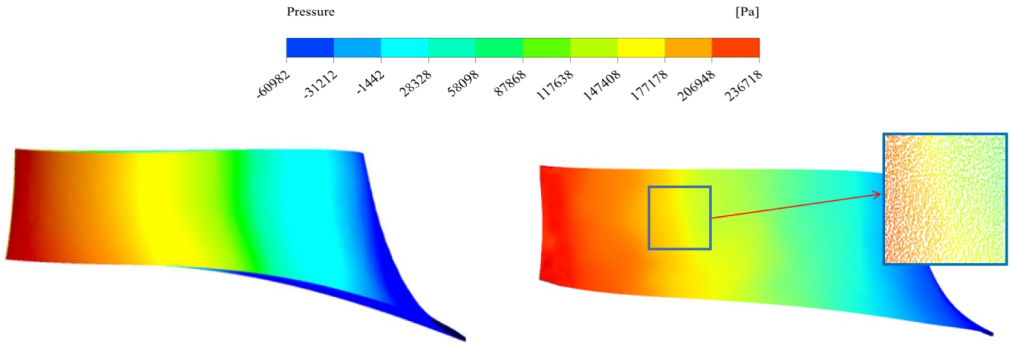

(a) CFD stress results. (b) Digital twin stress results.

Fig. 15 Comparison of CFD simulation and digital twin monitoring visualization

Within the VR environment module, users can utilize hardware devices to observe the force situation in areas such as the turbine wheel in a virtual reality environment.

Figure 15 illustrates a comparison between simulation outcomes from finite element software and stress monitoring results from the digital twin system under identical inputs. The graphical representation demonstrates that the distribution of stress monitoring cloud maps in the digital twin system closely aligns with CFD POST results, exhibiting even superior performance in pressure transition. With the implementation approach of the Open3d cloud map, errors are expected to remain within acceptable margins.

6 Conclusion

This study develops a pump-turbine monitoring system grounded in digital twin technology, which enhances operational and maintenance management, expands data dimensions, and advances the overall level of system intelligence. The key findings of this study are as follows:

(1) A five-dimensional model framework for pump-turbines, underpinned by digital twin technology, was designed, and a mechanical monitoring model utilizing the POD reduced-order model was constructed. The reliability of the reduced-order model was confirmed through an analysis of unit efficiency and pressure pulsation, demonstrating that the model's accuracy meets the required standards and significantly enhances solution efficiency.
(2) By integrating the POD reduced-order model with the LSTM pressure pulsation prediction algorithm, accurate predictions of pressure pulsation under complex conditions were realized, and the relationship between frequency-domain characteristics and cavitation was thoroughly investigated. A virtual twin was developed using the Unity3D platform, effectively coupling the physical and virtual systems through real-time data collection and transmission, achieving synchronization between physical and virtual domains, and offering a novel direction for the advancement of pump-turbine intelligence.
(3) The developed pump-turbine monitoring system was subjected to experimental testing, validating its feasibility in mechanical monitoring, fault prediction, and visualization. The user interaction proved effective, laying a solid foundation for realizing a highly advanced twin system capable of "controlling reality with virtuality" and "predicting reality with virtuality."

Acknowledgements This study received support from the National Natural Science Foundation of China under Grant Nos. 52066011.

Author contributions Qifei Li: conceptualization, methodology, software. Lu Xin: data curation, writing—original draft preparation. software, validation, writing—reviewing and editing. Runtao Li: visualization, investigation.

Data availability The authors are willing to provide the data upon reasonable request.

Declarations

Ethical approval and consent to participate Not applicable.

Competing interests The authors declare no competing interests.

References

1. Mei Z. Pumped storage power generation technology. Norwalk: Machinery Industry Press; 2000.
2. Li T. Pumped storage power stations. Water Resources and Hydropower Press. 1995.
3. Qiao Z. Discussion on the development issues and countermeasures of pumped storage power stations. Water Power New Energy. 2020;34(10):34–8.
4. Yang C. Study on selection and hydraulic stability of pumped storage units with ultra-high water head. Xi'an University of Science and Technology. 2017.
5. Li W, Li Z, Han W, et al. Time-mean equation and multi-field coupling numerical method for low-Reynolds-number turbulent flow in ferrofluid. Phys Fluids. 2023;35(12):125145.
6. Li W, Li Z, Han W, et al. Pumping-velocity variation mechanisms of a ferrofluid micropump and structural optimization for reflow inhibition. Phys Fluids. 2023;35(5): 052005. https://doi.org/10.1063/5.0149130.
7. Li W, Li Z, Han W, et al. Measured viscosity characteristics of Fe_3O_4 ferrofluid in magnetic and thermal fields. Phys Fluids. 2023;35(1): 012002. https://doi.org/10.1063/5.0131551.
8. Schluse M. From simulation to experimentable digital twins simulation-based development and operation of complex technical systems. 2016.
9. Shafto M, Conroy M, Doyle R, et al. Modeling, simulation, information technology and processing roadmap. Natl Aeronaut Sp Adm. 2012;32(2012):1–38.
10. Tao F, Liu W, Liu J, et al. Exploration of digital twins and their applications. Comput Integr Manuf Syst. 2018;24(1):1–18.
11. Knapp G, Mukherjee T, Zuback J, et al. Building blocks for a digital twin of additive manufacturing. Acta Mater. 2017;135:390–9.
12. Loureiro T, Rämä M, Sterling R, et al. District energy systems: a collaborative exchange of results on planning, operation and modelling for energy efficiency. Multidiscip Digit Publ Inst Proc. 2018;2(15):1127.
13. Sabri D, Ulf CM, Ivo S, et al. Online (remote) teaching for laboratory based courses using "digital twins" of the experiments. J Eng Gas Turbines Power. 2022;144: 051016.
14. Tao F, Zhang M, et al. Digital twin workshop—a new model for future workshop operations. Comput Integr Manuf Syst. 2017;23(1):1–9.
15. Tan F, Cheng J, Qi Q, et al. Digital twin-driven product design, manufacturing and service with big data. Int J Adv Manuf Technol. 2018;94:3563–76.
16. Qi Q, Tan F. Digital twin and big data towards smart manufacturing and industry 4.0: 360 degree comparison. IEEE Access. 2018. https://doi.org/10.1109/ACCESS.2018.2793265.
17. Tao F, Liu W, et al. Digital twin five-dimensional model and its applications in ten major fields. Comput Integr Manuf Syst. 2019;25(1):1–18.
18. Zhang Y, Qian C, Lv J, et al. Agent and cyber-physical system based self-organizing and self-adaptive intelligent shopfloor. IEEE Trans Industr Inf. 2017;13(2):737–47.
19. Zhang B, Meng Y, et al. Digital twin modeling and system implementation for assembly of complex components. 2023;9:37–44+60.
20. Broo G, Miguel A, et al. Design and implementation of a smart infrastructure digital twin. Autom Constr. 2022;136:104171–104171. https://doi.org/10.1016/j.autcon.2022.104171.
21. Guo Q, Tang F, et al. Five disruptive technologies in 6G to support digital twin networks. IEEE Wirel Commun. 2023. https://doi.org/10.1109/mwc.013.2200296.
22. Song H, Song M, et al. Online autonomous calibration of digital twins using machine learning with application to nuclear power plants. Appl Energy. 2022;326:119995–119995. https://doi.org/10.1016/j.apenergy.2022.119995.
23. Wang Z, Li S. Research on construction of digital twin pumped storage power stations. Water Resour Hydropower Express. 2023;44(9):110–5+122.
24. Yin G, Zhu G, et al. Monitoring system for shield machine tool changing robot based on digital twins [J/OL]. Comput Integr Manuf Syst. 2024. http://kns.cnki.net/kcms/detail/11.5946.TP.20230927.1149.012.html.
25. Shi S. Construction of digital twin for continuous casting equipment and research on remaining service life prediction method. Xi'an University of Science and Technology. 2023. https://doi.org/10.27398/d.cnki.gxalu.2023.001067.
26. Wang J, Liu Z, et al. Simulation evaluation of intelligent scheduling for tractor mixer assembly based on digital twins. Trans Chin Soc Agric Mach. 2024. p. 1–16.

27. Liu Q. Research and application of fault diagnosis method for centrifugal pump impeller mechanical based on digital twin technology. Lanzhou University of Technology. 2023. https://doi.org/10.27206/d.cnki.ggsgu.2023.000981.
28. Liu D, He L, Yang D, et al. Research progress on digital twin technology of human skeletal muscles. J Biomed Eng. 2023;40(4):784–91.
29. Zhou Y. Research on digital twin method of bridge structures and its application in state detection and performance evaluation. Chongqing Jiaotong University. 2021. https://doi.org/10.27671/d.cnki.gcjtc.2021.001100.
30. Zheng Y. Digital twin for geometric feature online inspection system of car body-in-white. Int J Comput Integr Manuf. 2021;34(7–8):752–63.
31. Wang Z. Towards next generation of pedestrian and connected vehicle in-the-loop research: a digital twin co-simulation framework. IEEE Trans Intell Veh. 2023;8(4):2674–83.
32. Hameed B, Khan I, Durr F, et al. An RFID based consistency management framework for production monitoring in a smart real-time factory. Internet of Things, Iot for a Green Planet, Tokyo. IEEE, 2010. p. 1–8.
33. Lee H. Framework and development of fault detection classification using Io T device and cloud environment. J Manuf Syst. 2017;43:257–70.
34. Zhuang J, Liu J, et al. Conntation, architecture and trends of product digital twin. Comput Integr Manuf Syst. 2017;23(04):753–68 (**in Chinese**).
35. Russo D, Rizzi C. Structural optimization strategies to design green products. Comput Ind. 2014;65(3):470–9.
36. Liu C. Analysis of coupled response of pumped storage unit under multiple physical fields and model reduction. Huazhong University of Science and Technology. 2022. https://doi.org/10.27157/d.cnki.ghzku.2022.000232.
37. Chen G, Li B, et al. Efficient coupled simulation of one-dimensional and three-dimensional thermal management of power battery pack. In: 2019 Annual Conference of Automotive Aerodynamics Branch of China Society of Automotive Engineers, Chongqing, China. 2019.
38. Golub GH, Van Loan CF. Matrix computations. 2nd ed. Baltimore: Johns Hopkins University Press; 1990.
39. Song M. Research on compound fault diagnosis method of crank-connecting rod mechanism in reciprocating compressor. Northeast Petroleum University. 2023. https://doi.org/10.26995/d.cnki.gdqsc.2023.001256.
40. Li Y, Sun L, et al. Study on transient flow and energy dissipation during turbine runner flyout process in mixed-flow turbine. J Hydraul Eng. 2023;54(07):794–805. https://doi.org/10.13243/j.cnki.slxb.20230079.
41. Tao R. Study on the influence of blade leading edge geometry characteristics on the inception cavitation of pump turbine. China Agricultural University. 2018.